Mechanics & Industry **16**, 112 (2015)

DOI: 10.1051/meca/2014072
www.mechanics-industry.org

Mechanics & Industry

Numerical analysis of cold-formed steel welded tube filled with concrete made of crystallized slag aggregate

Noureddine Ferhoune[1,a] and Jahid Zeghiche[2]

[1] Doctorate at civil engineering, University of Larbi Ben M'hidi Oum El Bouaghi, Algeria
[2] PhD Degree at civil engineering department, University of Al Baha, Saudi Arabia

Received 28 September 2013, Accepted 19 August 2014

Abstract – This paper presents a nonlinear finite element model to investigate the behaviour of cold-formed steel tubes filled with concrete made with crystallized slag aggregate. The columns had different lengths so that the length-to-depth ratio varied from 0.49 to 24. Nonlinear models for confined concrete and steel welded tubes with taking into account the effect of residual stress of steel section were used in the finite element model. The study was conducted over a wide range of concrete cylinder strengths from 20 to 45 MPa. The depth of flat portion-to-plate thickness (d/t) ratio hollow sections steel ranged from 24 to 52, covering compact and slender sections. The main studied parameters were: the section dimension and the effect of the in filled concrete and its age. The results obtained from the finite element analysis were verified against experimental results. An extensive parametric study was conducted to investigate the effects of cross-section geometry and concrete strength on the behaviour and strength of the columns. The column strengths obtained from the finite element analysis were compared with the design strengths calculated using the Eurocode 4.

Key words: Composite columns / concrete / cold-forming / finite element / structural design

1 Introduction

Concrete-filled steel tube columns have many advantages in terms of their high strength, high ductility, high stiffness and full usage of construction materials. In recent years, stainless steel tube members have become popular due to their high corrosion resistance, ease of construction and maintenance as well as aesthetic appearance. However, investigations of concrete-filled stainless steel tube columns are rarely found in the literature, especially using thin welded steel tubes. Tests of concrete-filled carbon steel tube columns were conducted by Schneider [1], Uy [2, 3], Huang et al. [4], Han and Yao [5], Mursi and Uy [6], and many other researchers. Hollow structural steel sections are often filled with concrete to form a composite column. Traditional concrete filled steel columns employ the use of hot rolled steel sections filled with concrete. These columns have been used wide spread as they speed up construction by eliminating formwork and producing high load carrying [7]. This leads to use small steel wall thickness and thus more economy. However, the major difficulty encountered is the local buckling of the steel wall especially in the case of stocky columns [8]. Very few experiments is done on built up cold formed welded steel sections filled with concrete or recycled materials [9] such as slag stone concrete designated here by SSC. The latter has been tested under direct compression and was used as a filling material to overcome the undesired effects of imperfections of built up cold formed sections. The gain in strength was found to reach a value of up to 2 and decreased linearly with the stubs height [9]. More test results are needed to indicate what would be the effect of the age of SSC on the behaviour and the load carrying capacity. No evidence is available in the literature to confirm the benefit of SSC age. The present work is a contribution to understand the behaviour of SSC filled cold formed thin short steel tubes subjected to axial compression.

Numerical modelling can be used to understand the behaviour of concrete-filled steel tube columns. However, developing an accurate model requires careful presentation of the concrete confinement, steel welded tube and steel tube-concrete interface. Hu et al. [11] developed a nonlinear finite element model using the ABAQUS program to simulate the behaviour of concrete-filled carbon steel tube columns. The concrete confinement was achieved by matching the numerical results by trial and error via parametric study. Roufegarinejad et al. [12] described a theoretical model for the behaviour and design

[a] Corresponding author:
ferhoune.noureddine@gmail.com

of concrete filled stainless steel columns subjected to axial compression and bending. Ellobody et al. [13] developed a nonlinear finite element model to investigate the behaviour of normal and high strength concrete-filled compact carbon steel tube circular columns. The concrete confinement was considered in the model.

The main objective of this study is to propose a nonlinear finite element model (nonlinear geometric and material) to investigate the behaviour and strength of cold-formed welded steel tube columns filled with concrete where the ordinary gravel was substituted by 10 mm crushed crystallized slag stone. Both rectangular hollow sections were investigated. The finite element program ABAQUS [14] was used in the analysis. A parametric study was performed to investigate the effects of concrete strength and cross-section geometry on the behaviour and strength of axially loaded concrete-filled cold-formed and welded steel tube columns. The column strengths obtained from the parametric study were compared with the design strengths calculated using the general design guides specified in the Eurocode 4 [15]. The results obtained from the model were verified against the test results conducted by Beggas [16], Zeghiche et al. [17], Ferhoune et al. [18].

2 Summary of experimental investigation

The experimental investigation of columns made with concrete-filled and welded section by Beggas et al. [16] provided the experimental ultimate loads of columns subjected to uniform axial compression. The columns had rectangular section; the studied section was made of two cold formed steel plates with U shape and welded to form a steel box. The cross section dimensions were: $100 \times 70 \times 2.0$ mm. The test program consisted of two test series. The first series of concrete-filled tubes, steel section is formed by welding the U shape in the large dimension (CWL100, CWL150, CWL200, CWL300, CWL400, and CWL500). In the second series tests by Beggas et al., the steel section is formed by welding the U shape in the small dimension (CWS100, CWS150, CWS200, CWS300, CWS400, and CWS500). The section size ($H \times B \times t$) of two series is $100 \times 70 \times 2$ mm and the stubs height varied from 100 mm to 500 mm. The concrete core is made with crystallized slag aggregate and concrete cylinder strengths at 28 days are 20 MPa. The crystallized slag does not influence at all the overall behavior of composite stubs, but the purpose of replacement of ordinary aggregate by crystallized slag aggregate is to exploit the waste of iron in the composition of concrete in order to obtain a concrete with same resistance at 28 days and, behavior compared with ordinary concrete.

In the cases of tests conducted by Zeghiche et al. [17] the columns had a rectangular section made with cold-formed steel and the value of concrete core cylinder strength at 28 days is 40 MPa, the steel dimensions ($H \times B \times t$) are $120 \times 80 \times 5$ mm (PR1, PR2, PR3, PR4, PR5, PR6, PR7). The columns height is 2760 mm and is

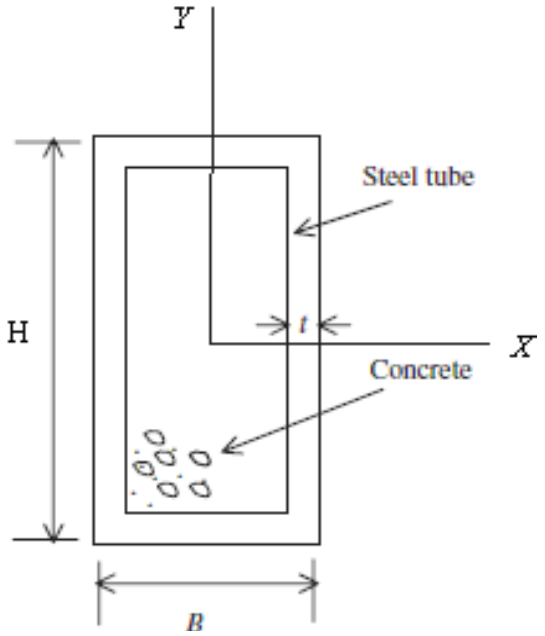

Fig. 1. Definition of symbols for concrete-filled rectangular hollow section specimens.

Table 1. Values of eccentricity in the cases of tests conducted by Zeghiche et al. [17].

Stubs N°	Eccentricity along (XX) e_X (mm)	Eccentricity along (YY) e_Y (mm)
PR1	0	0
PR2	24	0
PR3	60	0
PR4	0	16
PR5	0	40
PR6	24	16
PR7	60	40

subjected to eccentric load compression. For the tests conducted by Ferhoune et al. [18] (P1/3, P2/3, P3/3, P4/3), columns have a rectangular section made with steel box section (formed by U section steel and welded) filled with concrete. The section size ($H \times B \times t$) of two series is $100 \times 70 \times 2$ mm and the stubs height varied from 100 mm to 500 mm. The concrete core is made with crystallized slag aggregate and concrete cylinder strengths at 3 years of conservation are 30 MPa. The values of eccentricity in the case of test conducted by Zeghiche et al. [17] are presented in Table 1 and all geometric material characteristics are presented in Table 2.

3 Finite element model

3.1 General

There are four main parameters that need to be considered to simulate the actual behaviour of concrete filled rectangular hollow section and square hollow section steel tube columns, as shown in Figure 1. These parameters are

Table 2. Measured dimensions and material properties.

Stubs N°	B (mm)	H (mm)	t (mm)	L (mm)	H/t	L/H	f_y (MPa)	σ_{b28} (Mpa)
CWS100	68	102	2	100	51	0.98	300	20
CWS150	68	104	2	150	52	1.44	300	20
CWS200	68	102	2	200	51	1.96	300	20
CWS300	68	103	2	300	51.5	2.91	300	20
CWS400	67	102	2	400	51	3.92	300	20
CWS500	67	102	2	500	51	4.90	300	20
CWL100	74	98	2	100	49	1.02	300	20
CWL150	73	98	2	150	49	1.53	300	20
CWL200	74	95	2	200	47.5	2.11	300	20
CWL300	74	95	2	300	47.5	3.16	300	20
CWL400	75	95	2	400	47.5	4.21	300	20
CWL500	75	97	2	500	48.5	5.15	300	20
P1/3	72	99	2.40	196	41.25	1.98	295	30
P2/3	71	100	2.5	295	40	2.95	295	30
P3/3	68	98	2.3	390	42.61	3.98	295	30
P4/3	70	98	2.3	490	42.61	5	295	30
PR1	80	120	5	2760	24	23	386.3	44
PR2	80	120	5	2760	24	23	386.3	40
PR3	80	120	5	2760	24	23	384.7	40
PR4	80	120	5	2760	24	23	384.7	44
PR5	80	120	5	2760	24	23	343.3	43
PR6	80	120	5	2760	24	23	343.3	45
PR7	80	120	5	2760	24	23	357.5	44

the confined concrete, the steel tube, the welded section and the interface between the concrete and the steel tube. In addition to these parameters, the choice of the element type and mesh size that provide accurate results with reasonable computational time is also important to simulate the composite columns.

3.2 Finite element type and mesh

The 4-noded doubly curved shell elements with reduced integration S4R are used to model the buckling behaviour of the steel tube. The S4R element has six degrees of freedom per node and provides accurate solution to most applications. The element allows transverse shear deformation, which is important to simulate thick shell elements. The element also accounts for finite strain and is suitable for large strain analysis.

Fine mesh of three-dimensional 8-Node solid elements (C3D8) is used to model the concrete infilled. The nodes of welded zone formed by two U shapes are modelled by element called in library of ABAQUS Weld Connector. Different mesh sizes have been tried to choose the reasonable mesh that provides both accurate results and less computational time.

3.3 Boundary conditions and load application

Following the testing procedures conducted by Beggas et al. [16], Ferhoune [18] and Zeghiche [17], the top and bottom surfaces of the concrete filled cold-formed steel tube columns were restrained against all degrees of freedom, except for the displacement at the loaded end, which is the top surface, in the direction of the applied load, as shown in Figure 2. Other nodes were free to displace in all directions. The load was applied in increments using the modified RIKS method available in the ABAQUS library. In the case of axial compression (tests conducted by Beggas et al. [16], Ferhoune [18]), the load was applied as static uniform load using the displacement control at each node of the loaded top surface, which is identical to the experimental investigation. But in the situation of tests conducted by Zeghiche et al. [17], the eccentric load was concentrated in the position of eccentricity along (xx) axis or along (yy) axis by the intermediary of a steel plate (15 mm of thickness) and of large rigidity welded in the top and bottom surface, which is identical to the experimental investigation conducted by the author (Fig. 3).

3.4 Material modelling of high strength stainless steel tubes

The measured stress-strain curves obtained from tensile coupon tests presented by Beggas et al. [16] and Ferhoune [18] for rectangular and square cold-formed strength steel tubes have been used in the finite element analysis. The material behaviour provided by ABAQUS [14] (using the PLASTIC option) allowing for a nonlinear stress-strain curve has been used. The first part of the nonlinear curve representing the elastic part up to the proportional limit stress, with values of Young's modulus equal to 1.9×10^5 MPa and Poisson's ratio equal to 0.3, were used in the finite element model. To hold into account the effect of residual stress caused by geometric defect of steel section, the yield stress of steel section was

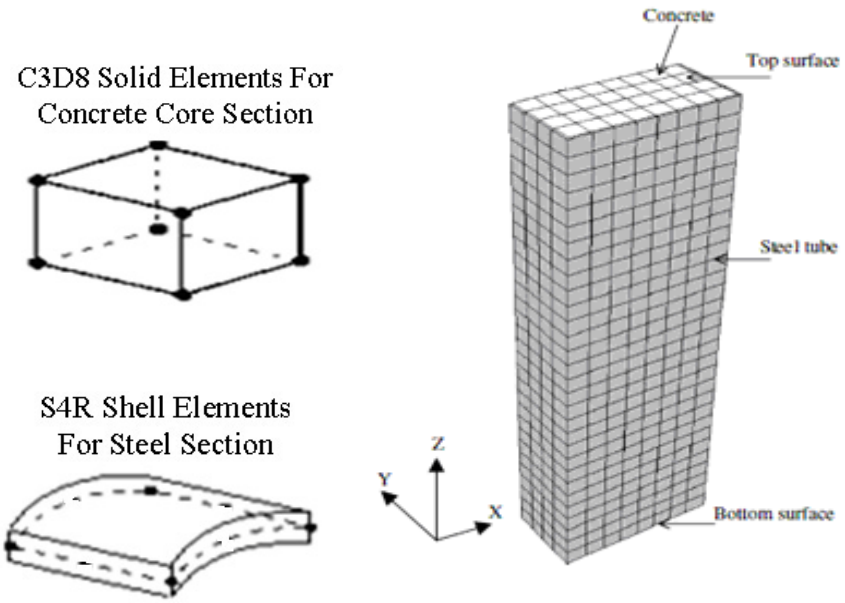

Fig. 2. Finite element mesh of concrete-filled rectangular steel tube columns.

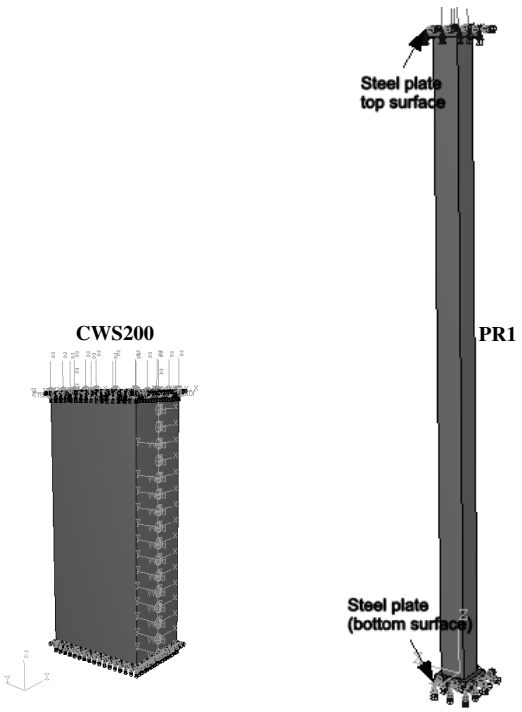

Fig. 3. Boundary conditions and load application, example of columns CWS200 and PR1.

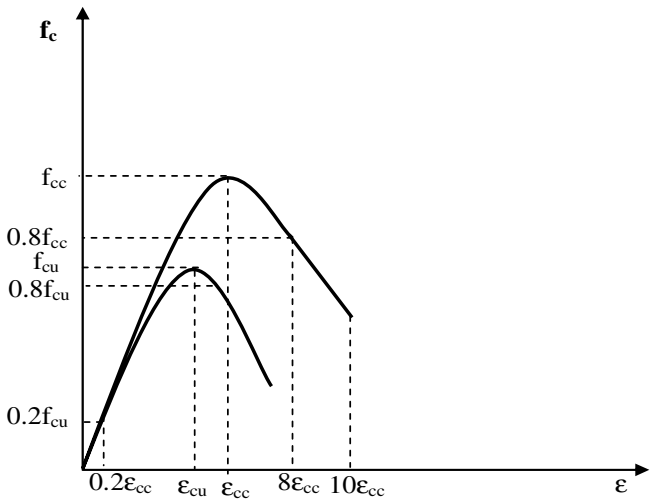

Fig. 4. Equivalent uniaxial stress-strain curves for confined and unconfined concrete.

penalized of 2% (it is has to say that the value of yield stress taken in the model is $0.98f_y$).

3.5 Modelling of confined concrete

Concrete-filled square hollow section and rectangular hollow section steel tube columns with large value of the overall depth of the steel tube-to-plate thickness (H/t) ratio provide inadequate confinement for the concrete. This is attributed to the premature failure of the columns due to local buckling of steel tubes. On the other hand, concrete-filled SHS and RHS steel tube columns with small value of H/t ratio provide remarkable confinement for the concrete. In this case, the concrete strength is considerably improved and the concrete model can be assumed as confined concrete model. In this study, it is intended to develop a confined concrete model and compare with experimental results. Figure 4 shows equivalent uniaxial presentation for the stress-strain curves of both unconfined and confined concrete, where f_c is the unconfined concrete cylinder compressive strength which is equal to $0.8(f_{cu})$, and f_{cu} is the unconfined concrete cube compressive strength. The corresponding unconfined strain

(ε_c) is taken as 0.003 as recommended by the ACI Specification [19]. The confined concrete compressive strength (f_{cc}) and the corresponding confined strain (ε_{cc}) can be determined from Equations (1) and (2), respectively, proposed by Mander et al. [20]

$$f_{cc} = f_c + k_1 f_l \tag{1}$$

$$\varepsilon_{cc} = \varepsilon_c \left(1 + k_2 \frac{f_l}{fc}\right) \tag{2}$$

where f_l is the lateral confining pressure imposed by the steel tube. The lateral confining pressure (f_l) depends on the H/t ratio and the steel tube yield stress (f_y). The approximate value of (f_l) can be interpolated from the measured values given by Hu et al. [11]. The value of (f_l) has significant effect for steel tubes with small H/t ratio. On the other hand, the value of (f_l) is equal to zero for steel tubes with H/t ratio greater than or equal to 29.2. The factors (k_1) and (k_2) are taken as 4.1 and 20.5, respectively, as given by Richart et al. [21]. Knowing (f_l), (k_1) and (k_2), the values of equivalent uniaxial confined concrete strength (f_{cc}) and the corresponding confined strain (ε_{cc}) can be determined using Equations (1) and (2). To define the full equivalent uniaxial stress-strain curve for confined concrete as shown in Figure 3, three parts of the curve have to be identified. The first part is the initially assumed elastic range to the proportional limit stress. The value of the proportional limit stress is taken as $0.8(f_{cu})$, while the initial Young's modulus of confined concrete (E_{cc}) is reasonably calculated using the empirical Equation (3) given by ACI [19].

$$E_{cc} = 4700\sqrt{f_{cc}}\ \text{MPa} \tag{3}$$

The Poisson's ratio (ν_{cc}) of confined concrete is taken as 0.2.

The second part of the curve is the nonlinear portion starting from the proportional limit stress $0.8(f_{cu})$ to the confined concrete strength (f_{cc}). This part of the curve can be determined from Equation (4) which is a common equation proposed by Saenz [22].

$$f = \frac{E_{cc}}{(1+R+R_E-2)(\varepsilon/\varepsilon_{cc}) - (2R-1)(\varepsilon/\varepsilon_{cc})^2 + R(\varepsilon/\varepsilon_{cc})^3} \tag{4}$$

This equation is used to represent the multi-dimensional stress and strain values for the equivalent uniaxial stress and strain values. The unknowns of the equation are the uniaxial stress (f) and strain (ε) values defining this part of the curve. The strain values (ε) are taken between the proportional strain, which is equal to ($0.8f_{cu}/E_{cc}$), and the confined strain (ε_{cc}), which is corresponding to the confined concrete strength. The stress values (f) can be easily determined from Equation (4) by assuming the strain values (ε).

Where RE and R values are calculated from Equations (5) and (6), respectively:

$$R_E = \frac{E_{cc}\varepsilon_{cc}}{f_{cc}} \tag{5}$$

$$R = \frac{R_E(R\sigma - 1)}{(R\varepsilon - 1)^2} - \frac{1}{R\varepsilon} \tag{6}$$

while the constants Rs and Re are taken equal to 4 as recommended by Hu et al. [11]. The third part of the confined concrete stress-strain curve is the descending part from the confined concrete strength (f_{cc}) to a value lower than or equal to ($r.k3.f_{cc}$) with the corresponding strain of $10\varepsilon_{cc}$. The reduction factor (k_3) depends on the H/t ratio and the steel tube yield stress (f_y). The approximate value of k_3 can be calculated from empirical equations given by Hu et al. [11]. The value of reduction factor (r) is taken as 1.0 for concrete with cube strength (f_{cu}) less or equal to 30 MPa. While, the value of r is taken as 0.5 for concrete with f_{cu} greater than or equal to 100 MPa, as recommended by Mursi and Uy [6]. The yielding part of the confined stress-strain curve for concrete, which is the part after the proportional limit stress, is treated by the Drucker Prager yield criterion model available in ABAQUS material library. The model is used to define yield surface and flow potential parameters for materials subjected to triaxial compressive stresses. The two parameters (Drucker Prager and Drucker Prager Hardening) are used to define the yield stage of confined concrete. The linear Drucker Prager model is used with associated flow and isotropic rule. The material angle of friction (β) and the ratio of flow stress in triaxial tension to that in compression (K) are taken as 20° and 0.8, respectively, as recommended by Hu et al. [11].

3.6 Modelling of concrete-steel tube interface

The contact between the steel tube and the concrete is modelled by interface elements. The interface elements consist of two matching contact faces of steel tube and concrete elements. The friction between the two faces is maintained as long as the surfaces remained in contact. The coefficient of friction between the two faces is taken as 0.25 in the analysis. We use the penalty function form for the friction contact between concrete and steel, in this method the contact term is given by

$$\Pi = \frac{1}{2}\text{kg}^2 \tag{7}$$

where k is a penalty parameter. The matrix equation for a nodal pair is now given by

$$\begin{bmatrix} k & -k \\ -k & k \end{bmatrix} \begin{Bmatrix} d\tilde{u}_2^s \\ d\tilde{u}_2^m \end{Bmatrix} = \begin{Bmatrix} -kg \\ kg \end{Bmatrix} \tag{8}$$

g is the gap given by Equation (9), where s signifies slave body and m master body

$$g = \tilde{x}_2^s - \tilde{x}_2^m \tag{9}$$

Thus, the solution of each contact constraint is treated as

$$g = \begin{cases} > 0; \text{ no contact} \\ 0; \text{ contact} \\ < 0; \text{ penetration} \end{cases} \quad (10)$$

The interface element allows the surfaces to separate under the influence of tensile force. However, both contact elements are not allowed to penetrate each other.

4 Strength design codes

EC4 (Eurocode 4) is the most recently completed international standard in composite construction. EC4 provided a simplified method of design for composite columns, which was based on the European buckling curves for the influence of instability and on cross section interaction curves determining the column section's resistance. EC4 covers concrete encased and partially encased steel sections and concrete-filled sections with or without reinforcement. Design procedure of the composite columns considers the second-order effects including imperfections and ensures that under the most unfavourable combinations of actions at the ultimate limit state, instability does not occur [15]. The plastic resistance to compression $N_{pl,Rd}$ of a composite cross-section was calculated by adding the plastic resistance of its components:

$$N_{pl.Rd} = A_a f_y/\gamma_{Ma} + A_c(0.85 f_{ck}/\gamma_c) + A_s f_{sk}/\gamma_s \quad (11)$$

where A_a, A_c and A_s are the cross-sectional areas of structural steel, concrete and reinforcement respectively; f_y, f_{ck} and f_{sk} are respectively the yield stress of steel cross section, the strengths of concrete and the yield stress of steel reinforcement ; γ_{Ma}, γ_c and γ_s are partial safety factors at the ultimate limit states.

5 Verification of finite element model

Recent experimental investigations on concrete-filled square hollow section steel tube columns conducted by Khandaker [18], as well as concrete-filled rectangular section steel tube columns conducted by Beggas et al. [16] and Zeghiche et al. [17] were used to verify the developed finite element model in this study. Table 2 summarizes the measured dimensions and material properties of the tested specimens. The test specimens conducted by Beggas [16] had nominal outer depth (H) and nominal length (L) of 95 mm, the column without concrete infilled having the plate thicknesses of 2.0 mm. The concrete cylinder strengths were 20 MPa and the yield stress of the steel tubes was 300 MPa. The nominal length-to-external high (L/H) ratio was 0.98. The nominal external depth-to thickness (H/t) ratio of the steel tubes was 47.5.

Concrete-filled rectangular hollow section steel tube test specimens conducted by Zeghiche et al. [17] had the steel tube plate thickness of 5.0 mm, depth of 80 mm and length of 2760 mm. Specimens PR1, PR4 and PR7 were concrete-filled rectangular hollow section steel tubes having concrete cylinder strengths of 44 MPa, and 40 MPa for specimens PR2 and PR2; columns PR5 and PR6 having concrete cylinder strengths of 43 and 45 MPa, respectively. The yield stress of the steel tubes was 386.3 MPa for columns PR1 and PR2, 384.7 MPa for PR3 and PR4, 343.3 MPa for PR5 and PR6 and 357.5 MPa for PR7. Concrete-filled rectangular hollow section steel tube test specimens conducted by Ferhoune [18] had the steel tube plate thickness varied from 2.3 mm to 2.5 mm and column lengths varied from 200 mm to 500 mm and width varied from 68 mm to 72 mm. The concrete cylinder strength is 30 MPa and the yield stress of steel is 300 MPa.

5.1 Comparison of finite element results with experimental results and design code EC4

A comparison between the experimental results and finite element results was carried out to verify the finite element model. The ultimate loads obtained from the tests (P_{Test}), finite element analysis (P_{FE}) and EC4 design code as well as the load-axial shortening curves and deformed shapes after failure have been investigated. Table 3 shows a comparison of the ultimate loads of the concrete-filled rectangular hollow section and square hollow section steel tube columns obtained experimentally, numerically using the finite element model and according EC4 code.

It can be seen that good agreement has been achieved between experimental results and finite element results for most of the columns. A maximum on estimate of load carrying capacity at 5% was observed between experimental and numerical results. Figure 4 shows the load-strain behaviour of concrete-filled rectangular hollow section steel tube series CWL. The experimental load was compared with the numerical prediction, and good agreement has been achieved. The specimens had the concrete cylinder strength of 20 MPa, depth varied from 100 mm to 500 mm and plate thickness of 2 mm. The column strength predicted using the finite element analysis varied from 291.3 kN to 238.3 kN, this load carrying capacity predicted by finite element method increases when the length decreases.

Different load-strain curves registered by using finite element model are presented in Figure 5. The finite element buckling mode in the case of tests conducted by Beggas et al. [16] is a convex local buckling as shown in Figure 6.

The strengths of the concrete-filled rectangular hollow section steel tube columns conducted by Ferhoune et al. [18] and the load-strain behaviour were obtained from the parametric study. The load-strain curves of the concrete-filled steel tube columns were plotted, as shown in Figures 7–10. It can be seen that the load of the columns decreases as the length increases. In this case of columns, the mode of buckling is a convex local buckling Figure 11.

In the case of concrete-filled rectangular hollow section steel tube columns conducted by Zeghiche et al. [17],

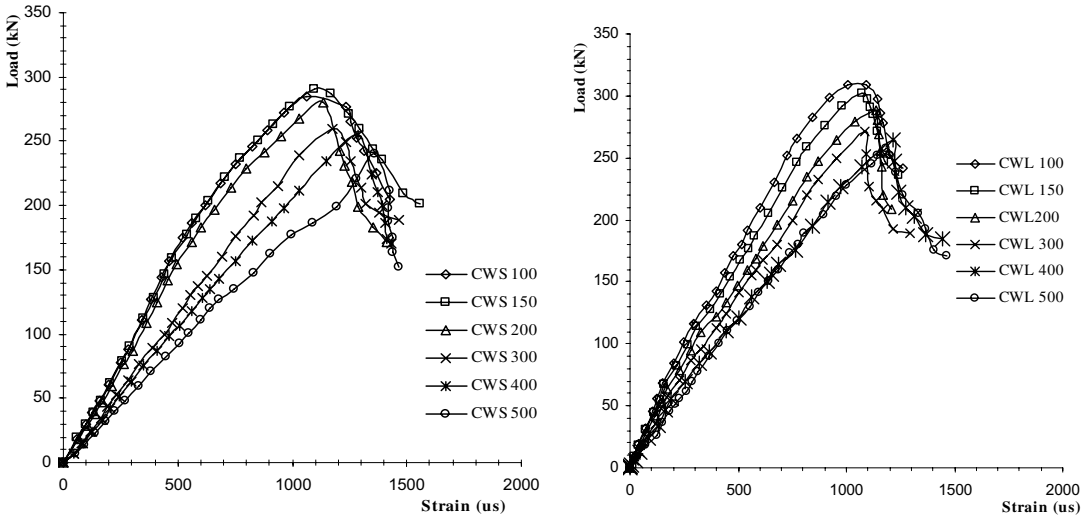

Fig. 5. Finite element results of series CWS and CWL.

Table 3. Comparison between tests, EC4 code and finite element analysis of concrete-filled steel tube column strengths.

Stub Reference	H/t	L/H	Test Load P_{Test} (kN)	FEM Load P_{EF} (kN)	EC4 P_{EC4} (kN)	$P_{\text{EF}}/P_{\text{Test}}$	$P_{\text{EC4}}/P_{\text{Test}}$
CWS100	51	0.98	290	291.3	306	1.004	1.050
CWS150	52	1.44	285	284.7	306	0.99	1.070
CWS200	51	1.96	270	266.4	306	0.98	1.130
CWS300	51.5	2.91	265	261.5	306	0.99	1.150
CWS400	51	3.92	250	246.1	306	0.98	1.220
CWS500	51	4.90	245	238.8	303	0.97	1.230
CWL100	49	1.02	310	309.5	268	0,99	0.860
CWL150	49	1.53	300	302.1	274	1.007	0.910
CWL200	47.5	2.11	290	288.7	270	0.99	0.930
CWL300	47.5	3.16	270	271.3	270	1.005	1.000
CWL400	47.5	4.21	265	264.7	273	0.99	1.030
CWL500	48.5	5.15	260	257.6	276	0.99	1.062
P1/3	41.25	1.98	347	323.8	302	0.93	0.870
P2/3	40	2.95	344	329.9	309	0.96	0.898
P3/3	42.17	4.02	349	303.7	301	0.90	0.888
P4/3	42.61	5	264	249.4	256	0.96	0.970
PR1	24	23	600	618	588.9	1.03	0.982
PR2	24	23	393	392.1	362.3	0,99	0.922
PR3	24	23	232	233.4	211.2	1.006	0.910
PR4	24	23	260	258.85	243.3	0.995	0.936
PR5	24	23	210	211.1	185.6	1.005	0.884
PR6	24	23	268	265.3	238.8	0.989	0.891
PR7	24	23	160	156.8	140.9	0.98	0.881

the mode of buckling is the general buckling according axis with weak rigidity when the load is concentred or when the eccentric load is applied in (xx) axis (column PR1, PR2 and PR3), and according with axis with strong rigidity when the eccentric load is applied in (yy) axis (column PR4 and PR5). But in the case of columns PR6 and PR7, the type of buckling is a general buckling according the two axes, with strong stressing according to the weak rigidity axis (xx) compared to the strong rigidity axis (yy). Figure 12 presents the example of numerical buckling mode of PR1 and PR6. The different results of load-strain curve at mid length of this series are presented in Figures 13–15.

The comparison between ultimate load strength calculated by EC4 design code and experimental results shows in the case of columns CWL100, CWL150, CWL200, and the series of stubs tested by Ferhoune et al. [18] and Zeghiche et al. [17], the EC4 prediction [15] a under-estimate of the load carrying capacity but it is on the safe side; the maximum percentage of under-estimation of load is 14% for columns CWL100. By the way, there is an overestimate of strength

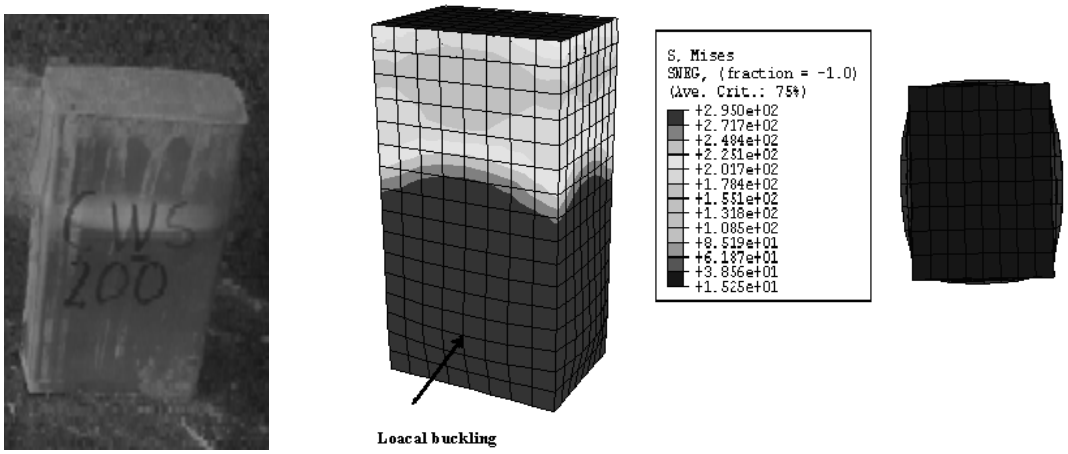

Fig. 6. Comparison of experimental and finite element analysis failure modes of specimen CWS200. (a) Experimental, (b) FE analysis.

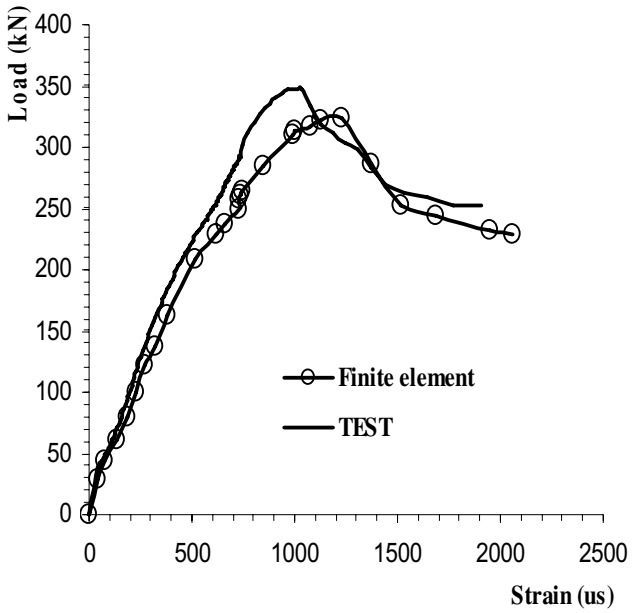

Fig. 7. Load-strain curve of column P1/3.

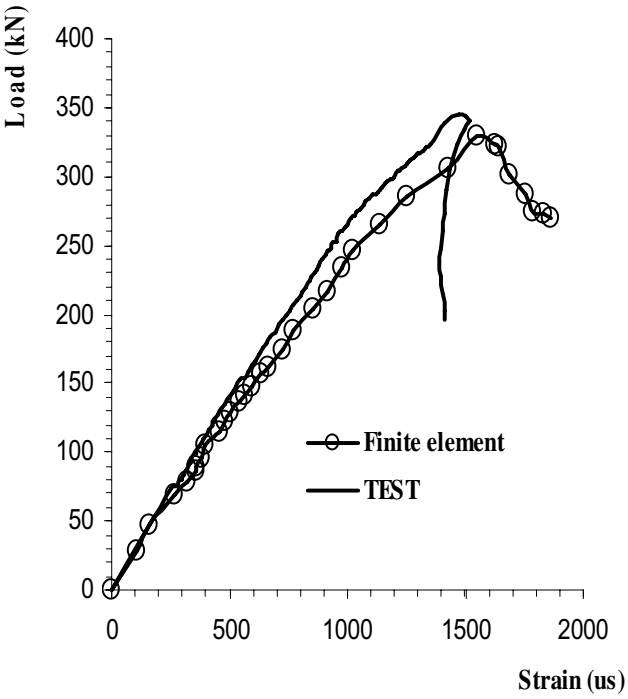

Fig. 8. Load-strain curve of column P2/3.

load according EC4 design compared with experimental load of columns EWS100, EWS150, EWS200, EWS300, EWS400, EWS500, CWL400, CWL500, the maximum percentage of overestimation of load is 23% for columns CWS500.

6 Discussion

This work presents a nonlinear finite element model to investigate the behaviour and design of axially loaded concrete filled with cold-formed steel tube columns. A comparison between experimental column load strength, finite element load and load carrying capacity calculated according Eurocode 4 designs of different columns is exposed. Figures 16 and 17 show the relationship between the column strengths and stubs height. The figures plotted the column strengths obtained from tests and the finite element analysis in comparison with that obtained from the design rules specified in the EC4 [15].

It can be seen that the column strengths increase as the stubs height decreases. It is also shown that the design rules specified in the EC4 generally overestimate the column strengths except the columns CWL200, CWL300 and CWL500. A good agreement of load carrying capacity is obtained between finite element prediction and test results in the case of columns CWS and CWL.

In the case of columns tested by Ferhoune et al., the mode of instability is a local buckling. The load carrying

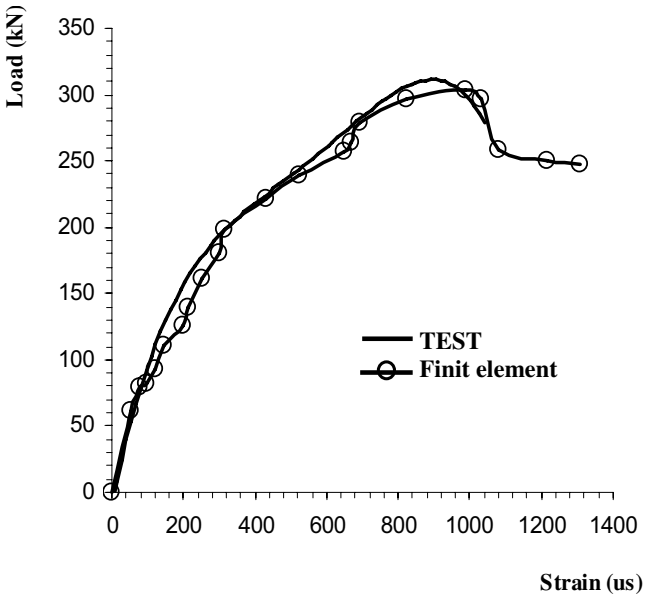

Fig. 9. Load-strain curve of column P3/3.

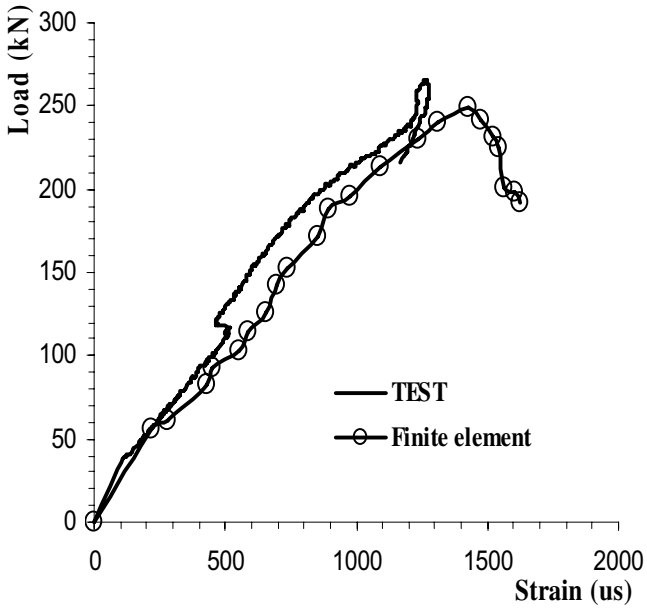

Fig. 10. Load-strain curve of column P4/3.

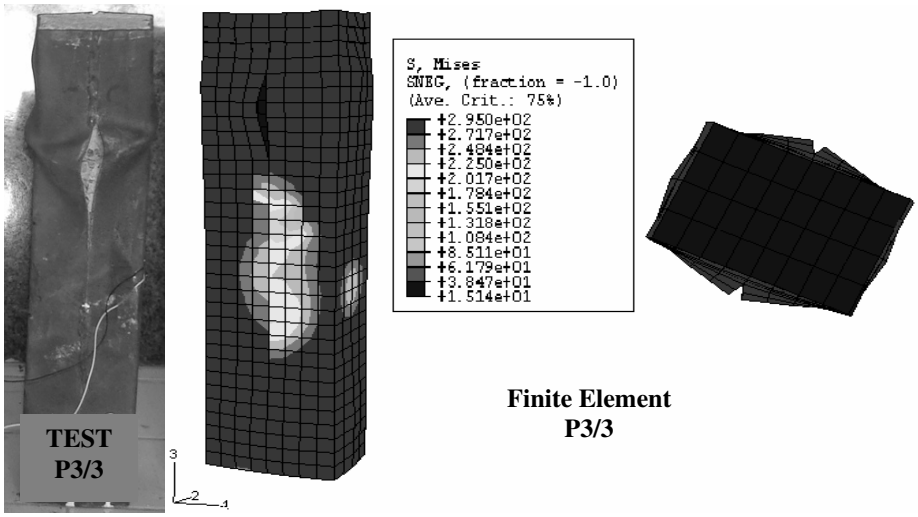

Fig. 11. Comparison of buckling mode between test and finite element of column P3/3.

capacity calculated according EC4 prediction and finite element method is under than the strength test but it is on safe side (Fig. 18).

The comparison between test load and finite element load of columns tested by Zeghiche et al. [17] shows a good agreement between them. The mode of instability in this case is a general buckling. The experimental, finite element and prediction failure loads according EC4 are plotted in Figures 19 and 20 against the eccentricity ratios e_x/H, e_y/B. in the case of major and minor axis bending. Figures 19 and 20 show that the EC4 predictions are on the safe side, as they are lower than experimental values. It can be seen that the finite element results in this cases are on the safe side compared with experimental results. The failure load increases as the eccentricity ratios decrease, the stressing of decreases load is less important in the cases of major axis bending compared with minor axis bending.

The experimental, finite element and prediction failure loads according EC4 [15] are plotted in Figures 19 and 20 against the eccentricity ratios e_x/H, e_y/B. in the case of major and minor axis bending. Figures 19 and 20 show that the EC4 predictions [15] are on the safe side, as they are lower than experimental values. It can be seen that the finite element results in these cases are on the safe side compared with experimental results. The failure load increases as the eccentricity ratios decrease, the stressing of decreases load is less important in the cases of major axis bending compared with minor axis bending.

Figure 21 shows the comparison between the experimental failure load, and the load carrying capacity calculated according EC4 prediction and finite element model

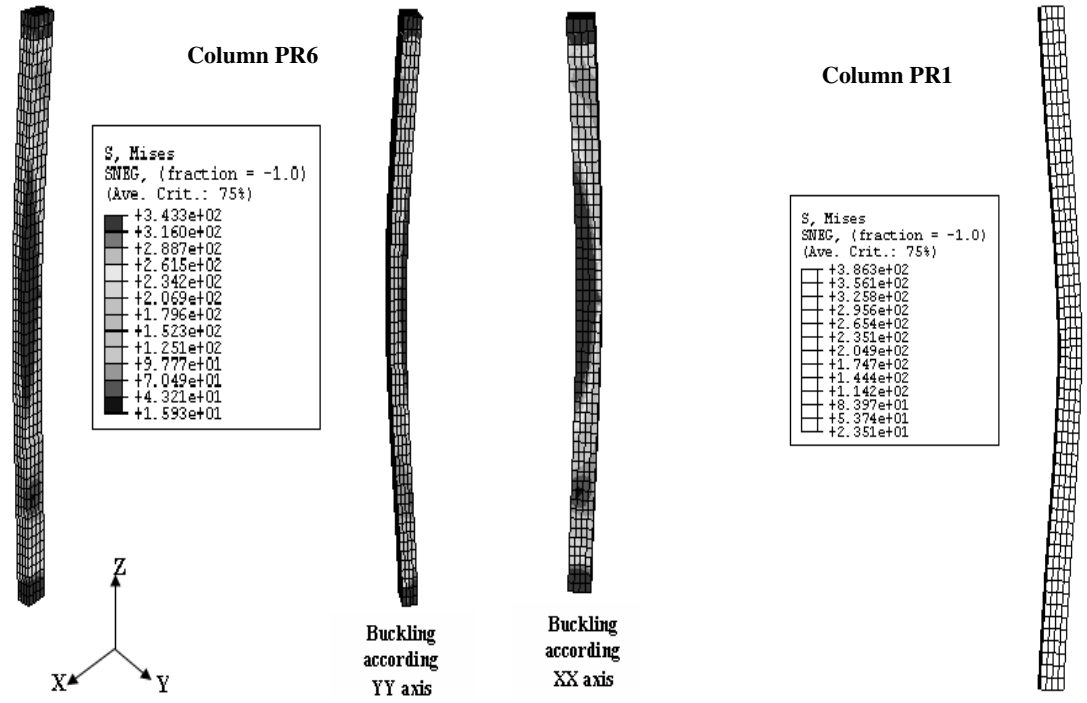

Fig. 12. Finite element analysis failure modes of column PR1 and PR6.

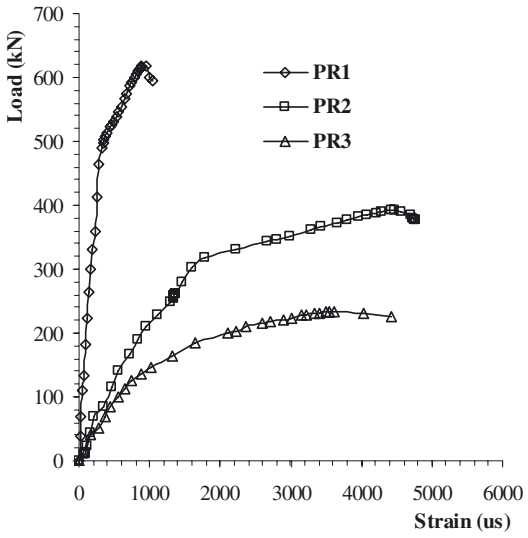

Fig. 13. Finite element load-strain curve of column subject to major axis bending.

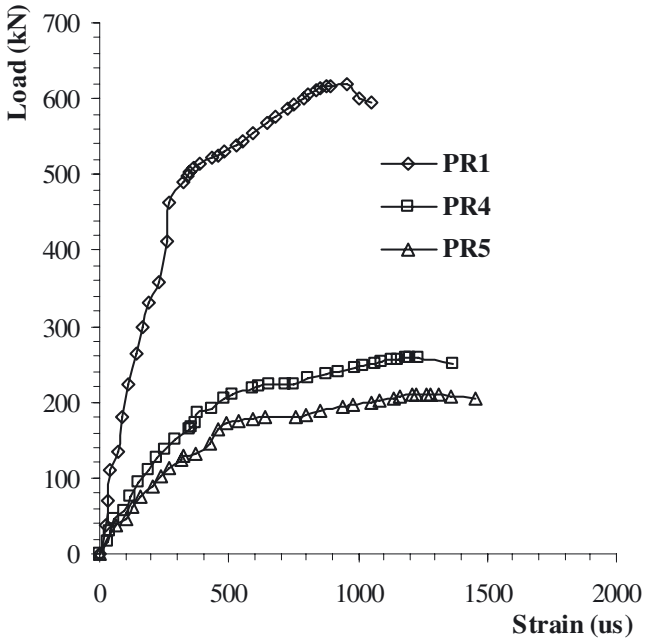

Fig. 14. Finite element load-strain curve of column subject to minor axis bending.

in function with double bending axis. It can be seen that a good agreement is obtained between finite element and experimental results. The EC4 design code [15] is on safe side in this case, but he under-estimate the load carrying capacity compared with experimental results, the maximum rate of under-estimation is for columns PR7 (11.9%), although it is on safe side.

Figure 22 plotted the relationship between the column strengths obtained from finite element analysis (P_{FE}) and tests (P_{Test}) for concrete filled square and rectangular hollow steel section. Generally, it can be seen that the proposed finite element model strengths are accurately predicted for concrete filled rectangular steel section with different H/t ratios. It can conclude that the relationship

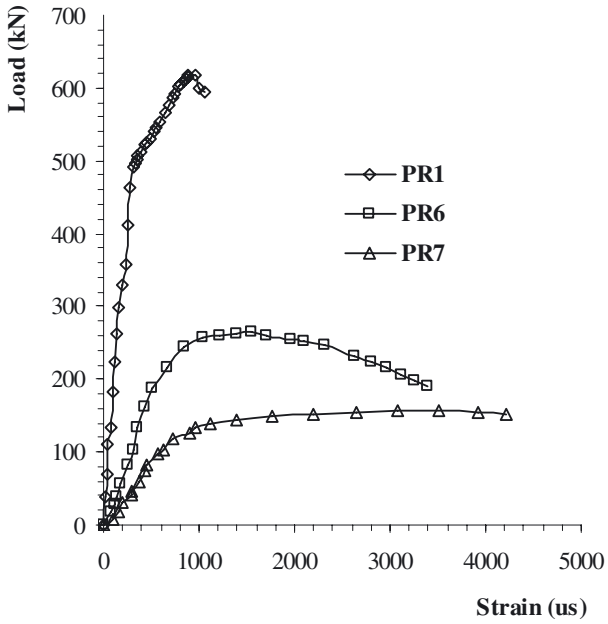

Fig. 15. Finite element load-strain curve of column subject to biaxial bending.

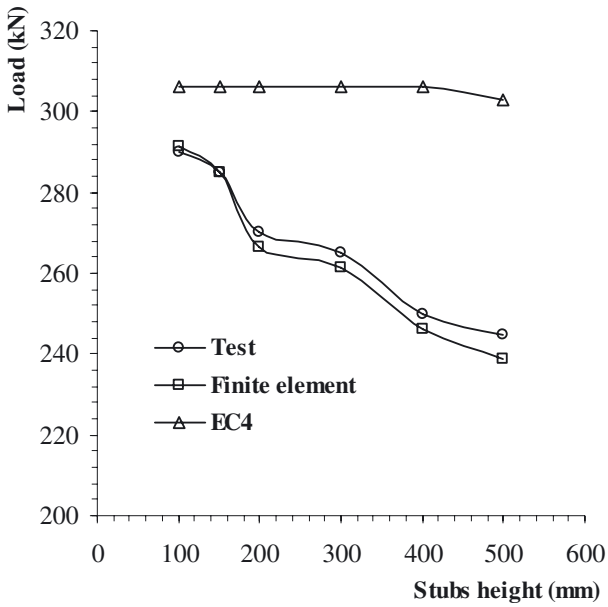

Fig. 16. Load-stubs height relation of CWS columns.

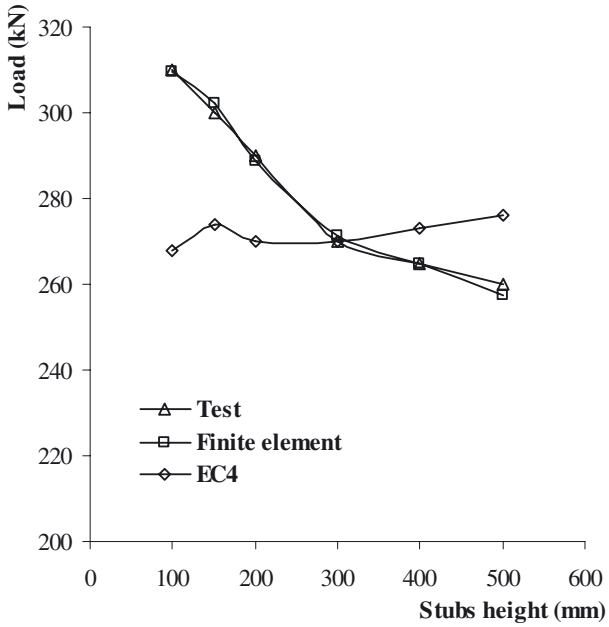

Fig. 17. Load-stubs height relation of CWL columns.

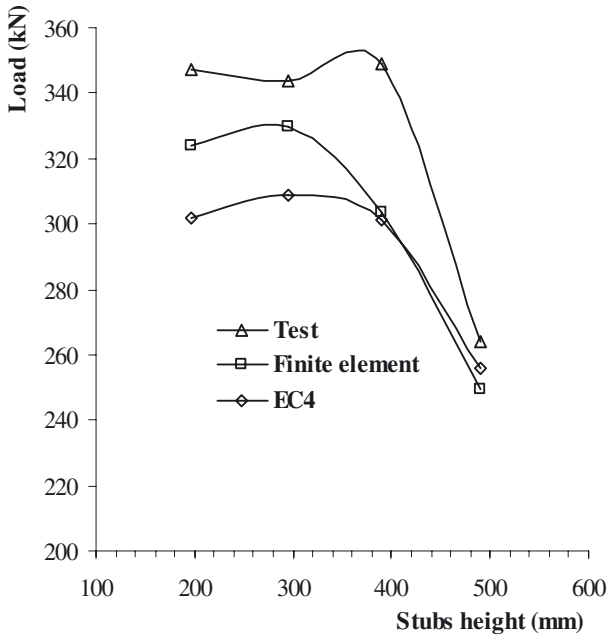

Fig. 18. Load-stubs height relation of series conducted by Ferhoune.

between P_{FE} and P_{Test} is linear and the equation of this relation is $Y = Ax + B$.

7 Conclusion

The paper presents an accurate nonlinear finite element model for the analysis of different strengths of concrete-filled rectangular steel tube columns. The confined concrete has been accurately modelled. The measured stress-strain curves of steel tubes were used to simulate the actual material properties. The comparison between the finite element results and the experimental results of the columns with different concrete strengths and different geometric dimensions showed good agreement in predicting the behaviour and strength of the columns. The columns strengths, load-axial shortening curves and deformed shapes of the columns have been predicted using the finite element model and generally compared well with the experimental results.

Parametric study of concrete-filled rectangular hollow section steel tube columns with different overall depths of the steel tube-to-plate thickness ratio ranged from 24 to

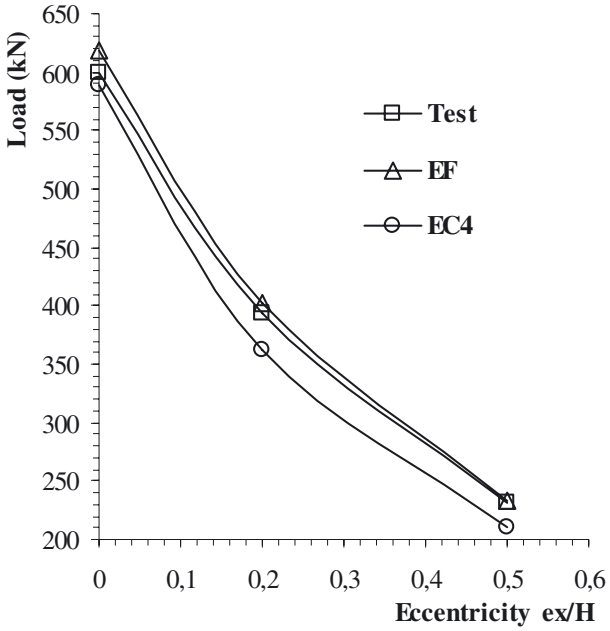

Fig. 19. Failure load according major axis bending (columns PR1, PR2 and PR3).

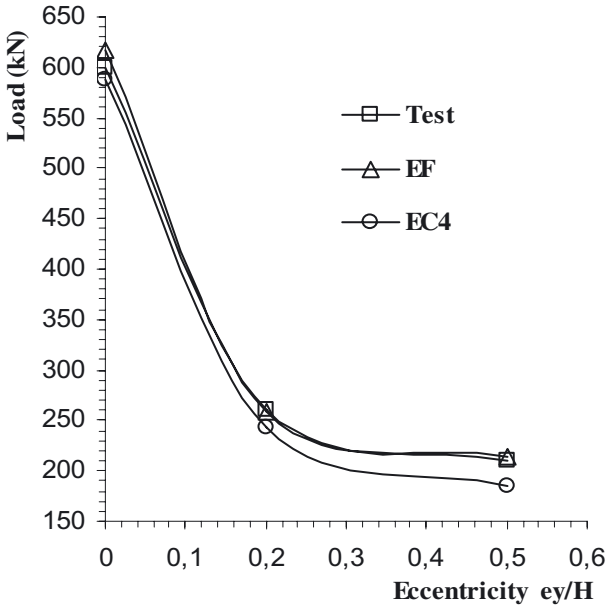

Fig. 20. Failure load according minor axis bending (columns PR1, PR4 and PR5).

52 and different concrete cube strengths ranged from 20 to 45 MPa was performed using the verified finite element model. The column strengths predicted from the parametric study using the finite element model was compared with the design strengths calculated using the EC4 code specifications. It is shown that the design strengths calculated using the European Code are on safe side, except for concrete-filled rectangular hollow section steel tube columns having the overall depth of the steel tube-to-plate thickness ratio greater than 49.

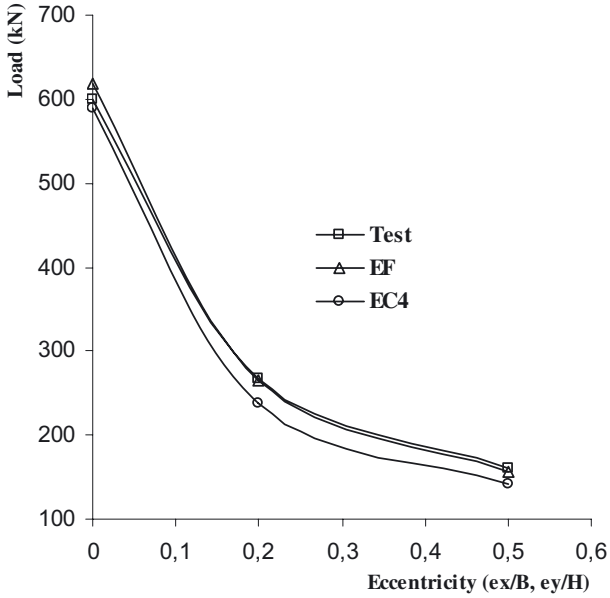

Fig. 21. Failure load according minor and major axis bending (Columns PR1, PR6 and PR7).

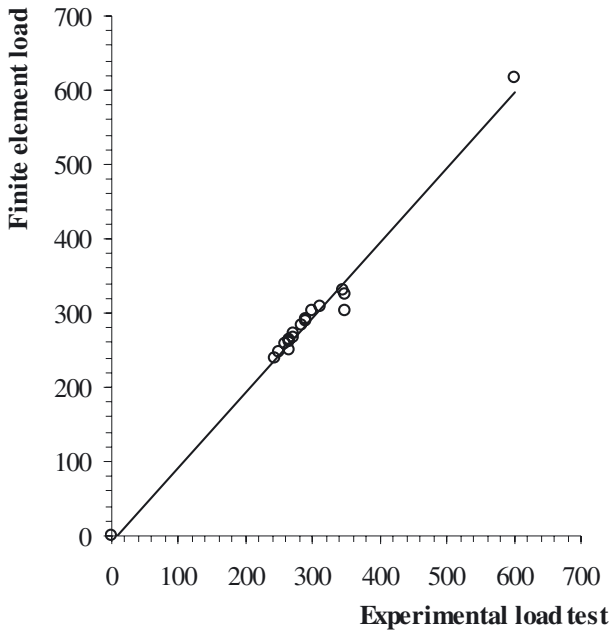

Fig. 22. Experimental load and Finite element load relation for concrete-filled rectangular steel tube columns subject to axial compression.

References

[1] S.P. Schneider, Axially loaded concrete-filled steel tubes, J. Struct. Eng. 124 (1998) 1125–1138

[2] B. Uy, Local and post-local buckling of concrete filled steel welded box columns, J. Construct. Steel Res. 74 (1998) 47–72

[3] B. Uy, Static long-term effects in short concrete-filled steel box columns under sustained loading, ACI Struct. J. 98 (2001) 96–104

[4] C.S. Huang, Y.K. Yeh, H.T. Hu, K.C. Tsai, Y.T. Weng, S.H. Wang et al., Axial load behavior of stiffened concrete-filled steel columns, J. Struct. Eng. 128 (2002) 1222–1230
[5] L.H. Han, G.H. Yao, Influence of concrete compaction on the strength of concrete-filled steel RHS columns, J. Construct. Steel Res. 59 (2003) 751–767
[6] M. Mursi, B. Uy, Strength of concrete filled steel box columns incorporating interaction buckling, J. Struct. Eng. 129 (2003) 626–639
[7] J. Zeghiche, Concrete filled steel tubes, Ph.D. thesis, University of Annaba, 2005
[8] Z. Bassam, S.G. Emhaidy, Enhancing filled-tube properties by using fiber polymers in filling matrix, J. Appl. Sci. 5 (2005) 232–235
[9] You-Fu Yang, Lin-Hai Han, Experimental behaviour of recycled aggregate concrete filled steel tubular columns, J. Construct. Steel Res. Article in press (2006)
[10] V.K.R. Kodur, Performance of high strength concrete-filled steel columns exposed to fire, Can. J. Civ. Eng. 25 (1998) 975–981
[11] H.T. Hu, C.H. Huang, M.H. Wu, Y.M. Wu, Nonlinear analysis of axially loaded concrete-filled tube columns with confinement effect, J. Struct. Eng. 129 (2003) 1322–1329
[12] A. Roufegarinejad, B. Uy, M.A. Bradford, Behaviour and design of concrete filled steel columns utilizing stainless steel cross sections under combined actions, In: Proceedings of the 18th Australasian conference on the mechanics of structures and materials, 2004, pp. 159–165
[13] E. Ellobody, B. Young, D. Lam, Behaviour of normal and high strength concrete-filled compact steel tube circular stub columns, J. Construct. Steel Res. (2005) (in press)
[14] ABAQUS Standard User's Manual, Version 6.4. Hibbitt, Karlsson and Sorensen, Inc., USA, 2004, Vol. 1–3
[15] Eurocode 4, Design of composite steel and concrete structures, part1.1: General rules and rules for buildings
[16] D. Beggas, Experimental squash load of concrete-filled thin welded cold formed steel stubs with different welding fillets location, Ph.D. thesis, University Badji Mokhtar, Annaba, 2009
[17] J. Zeghiche, Dr. H. Shakir-Khalil, Experimental behaviour of concrete-filled rolled rectangular hollow section columns, J. Instit. Struct. Eng. 346–353
[18] N. Ferhoune, J. Zeghiche, Experimental behaviour of concrete-filled rectangular thin welded steel stubs (compression load case), C.R. Mecanique 340 (2011) 156–164
[19] ACI, Building code requirements for structural concrete and commentary, ACI 318-99, American Concrete Institute, Detroit, USA, 1999
[20] J.B. Mander, M.J.N. Priestley, R. Park, Theoretical stress–strain model for confined concrete, J. Struct. Eng. 114 (1988) 1804–1826
[21] F.E. Richart, A. Brandzaeg, R.L. Brown, A study of the failure of concrete under combined compressive stresses. Bull. 185. Champaign, IL, USA: University of Illinois Engineering Experimental Station, 1928
[22] L.P. Saenz, Discussion of Equation for the stress-strain curve of concrete by P. Desayi, and S.J. Krishnan, Am. Concrete Inst. 61 (1964) 1229–1235